Vortices and Turbulent Relaxation in Magnetized Electron Columns

C.F. Driscoll, K.S. Fine, X.-P. Huang, T.B. Mitchell,† and B.P. Cluggish

Department of Physics and *Institute for Pure and Applied Physical Sciences*
University of California at San Diego, La Jolla, CA 92093 USA
fdriscoll@ucsd.edu

Abstract

Magnetically confined electron columns evolve as near-ideal 2D fluids, allowing quantitative study of shear flow instabilities, vortex formation, turbulence, and self-organization. We find that rapid global symmetrization of a distorted column can occur by a decay instability due to nonlinear beat wave damping. When instabilities lead to vortex turbulence which then freely relaxes, we find that the relaxation rate is limited by vorticity holes which persist for hundreds of rotations even in strong background shear. Long wavelength turbulence is observed to self-organize to a meta-equilibrium state which is accurately predicted by minimization of enstrophy, although relaxed states from shorter wavelength turbulence appear substantially different. Surprisingly the relaxation can be halted by the formation of "vortex crystals," where 3 to 12 vortices form a geometric lattice which is stable for up to 10^4 rotation times. After even longer times, a weak compressional viscosity arising from "rotational pumping" may contribute to 3D relaxation.

1. Introduction

Magnetically confined pure electron columns are excellent systems for observing 2D vortices, turbulence, and self-organization in the presence of background shear flow [1]. The electron columns are confined radially by a uniform magnetic field, B_z, and contained axially by voltages applied to end sections of the cylindrical wall, as shown in Fig. 1. The confined plasma is sensed and manipulated by antennas in the wall, and the z-averaged electron density $n(r,\theta,t)$ is accurately measured by dumping the column onto a phosphor screen imaged by a $512 \times 512 \times 16$ bit CCD camera.

The axial bounce frequency of an electron is large compared to the $\mathbf{E}\times\mathbf{B}$ drift rotation frequency ($\omega_B \gg \omega_R$), so the flow can be described by the 2D drift-Poisson equations, *i.e.*

$$\frac{\partial n}{\partial t} + \mathbf{v}\cdot\nabla n = 0\ ,\quad \mathbf{v} = -\frac{c}{B_z}\nabla\phi\times\hat{\mathbf{z}}\ ,\quad \nabla^2\phi = 4\pi e n\ . \tag{1}$$

These equations are isomorphic to the 2D Euler equations for an incompressible inviscid fluid, and are close cousins to the Hasegawa-Mima equations for drift-wave turbulence [2]. The measured electron density is proportional to the vorticity of the flow, *i.e.* $n = (B_z/4\pi ec)\,\nabla\times\mathbf{v}$.

The plasma column has low internal viscosity and has no boundary layers at the cylindrical walls or ends. For electrons the time for internal viscosity to act is typically 10 sec [3], compared to the 10 μsec time scale for the fastest drift motions. Further, the

† Present address: Los Alamos National Laboratory, K-480, P.O. Box 1663, Los Alamos NM 87545.

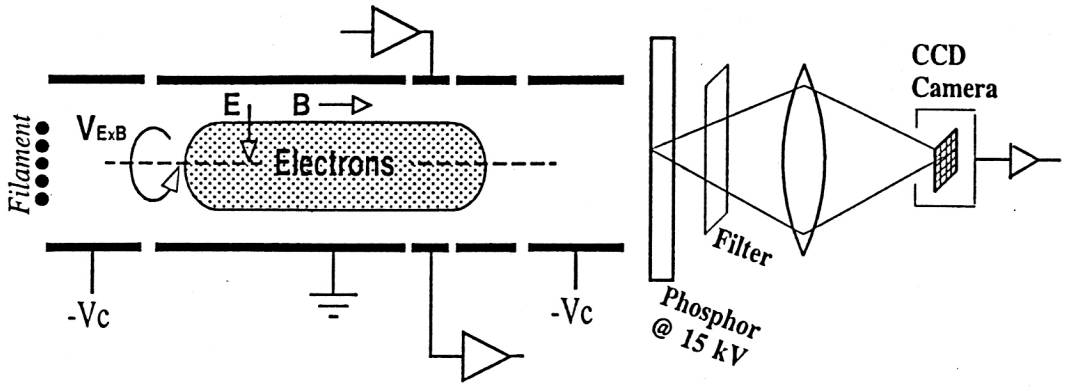

FIG. 1. The cylindrical confinement geometry and phosphor/camera diagnostic.

$\mathbf{E}\times\mathbf{B}$ drift velocity v_θ may be large at the wall, but since there are typically no particles near the walls, one has a free-slip boundary condition. The effects of compressional viscosity acting on rotational pumping of the length of the plasma will be considered below.

2. Shear Flow Modes and Instabilities

If we start with a smooth, symmetric density profile $n(r)$ and add a small perturbation in θ, we are able to study near-linear modes and instabilities. Our $n(r,\theta,t)$ data allows us to completely characterize the $k_z = 0$ flute modes, varying as $\exp(im\theta - i\omega_m t)$. When the electron density profile $n(r)$ is monotonically decreasing, an azimuthally symmetric column is stable with respect to all $\mathbf{E}\times\mathbf{B}$ drift modes. When surface modes are excited, we observe direct and beat-wave damping of the mode. For hollow profiles, we observe both the expected Kelvin-Helmholtz instabilities and other stable $\mathbf{E}\times\mathbf{B}$ drift, or ''diocotron'' modes.

Similar flute modes have been extensively analyzed [4] and have recently been observed in neutral plasmas with electric fields arising from regions of non-neutrality [5,6]. One interesting question is the net charge of the plasma and the effects of image charges in the walls. For cylindrical geometry, the image charges from a net plasma charge give rise to the stable $m = 1$ diocotron mode, wherein the entire displaced plasma column orbits around the center of the confinement cylinders. For toroidal geometry, this image charge mode would be more complicated.

These diocotron modes modes in electron plasmas are not well-predicted by the usual step-profile analysis: distinct stable and unstable modes are observed experimentally, whereas theory predicts complex conjugate pairs. However, both the frequencies and growth rates are reasonably well characterized by computational solution of the eigenvalue equation using the measured density profiles [7]. A further exception is $m = 1$, where we observe a robust exponential instability [8] where cold fluid theory predicts only algebraic growth; here, FLR and finite length effects may cause the instability [9].

The damping of these modes can not be obtained from step-profile analysis of $n(r)$, since this idealization precludes resonance between the wave and the fluid rotation at a radius where the vorticity is not spatially constant [10]. This ''direct'' resonance is now understood to give rise to inviscid spatial Landau damping of the wave [11], analogous to velocity space Landau damping of electron plasma waves. The resonance is centered at r_s, where $\omega_m = m\,\omega_R(r_s)$. For even moderate wave amplitudes, this observed damping is typically nonlinear, and the damping may decrease [12] or cease when the resulting ''cat's-eye'' flows generate fine-scale filaments inside the vortex. For ''sharp-edged'' vorticity profiles, the resonant radii r_s can be completely outside the vortex, in which case no direct resonance damping occurs.

For general vorticity profiles, however, we find [13] that a single excited wave varying as $A_m \sin(m\theta)$ will decay into a daughter wave varying as $A_{m-1}\sin[(m-1)\theta]$, through resonance damping of the nonlinear "beat wave" at frequency $\omega_m - \omega_{m-1}$. Here, the resonance is where $\omega_m - \omega_{m-1} = \omega_R(r_s)$. The daughter mode is oberved to grow exponentially, at a rate varying roughly as A_m^2. These rates (normalized by τ_R) are shown in Fig. 2 for mode numbers $4 \rightarrow 3$, $3 \rightarrow 2$ and $2 \rightarrow 1$. Also shown is an initial large amplitude $m = 3$ state and the $m = 2$ state which results $10\,\tau_R$ later.

When the resonant coupling exists, a single surface wave is an unstable equilibrium, and no equilibrium exists with two waves. One consequence of this beat-wave damping is that a long-wavelength mode (such as an $m = 2$ elliptical distortion) would appear to actively damp or suppress shorter wavelength modes such as $m = 3$. This decay process is seen to give global symmetrization of an asymmetric vortex, while presumably also generating fine-scale resonance filaments within the vortex. For many vortex profiles, this beat wave damping is observed to be the fastest mechanism for symmetrization. Further, shape distortions are an inherent result of vortex-vortex interactions [14], including those leading to merger [15] or filamentation, so direct damping and beat-wave damping may affect these interaction processes.

3. Relaxation of Fluctuations in Shear

We study instabilities and relaxation by creating well-controlled but unstable initial conditions and then observing the free evolution. Shear-flow instabilities lead to the formation of vortices, which result in rapid cross-field particle transport to a state which is no longer globally unstable. The vortices then merge, shed filaments, and eventually relax to an

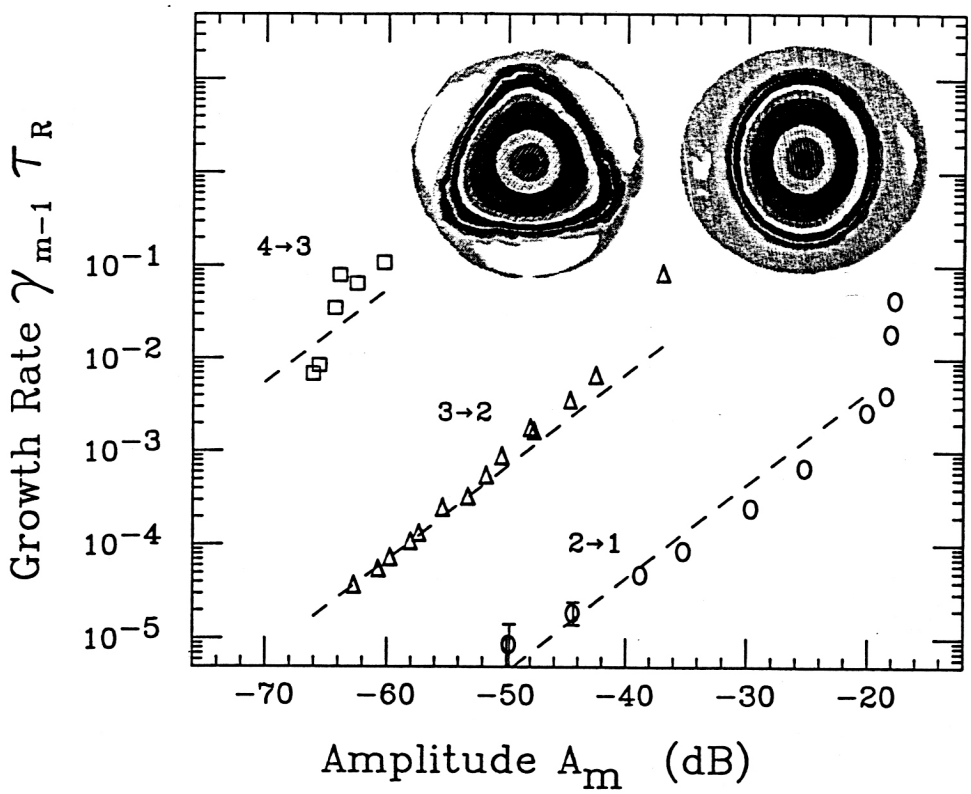

FIG. 2. Measured decay instability growth rates $\gamma_{m-1}\tau_R$ versus mode amplitude A_m, for $m = 4$, 3 and 2. Insert shows $n(r,\theta)$ before and after the $3 \rightarrow 2$ instability.

axisymmetric, sheared meta-equilibrium state. This state can be treated as a sheared θ-averaged background profile, plus turbulent fluctuations on various spatial scales. An example of such an evolution is shown in Fig. 3.

We find that measured fluctuations decay about 50 times slower than predicted by simple "passive tracer mixing" in the presence of shear, and that the measured "noise" is strongly skewed from Gaussian [16]. These effects are due to the longevity of "holes," *i.e.* self-trapped regions of negative relative electron density or vorticity. These holes are clearly visible in the fourth and fifth frames of Fig. 3. Figure 4 shows the shot-to-shot density fluctuations $\tilde{n}$ measured at $r \equiv R/R_w = 0.33$. The fluctuations are observed to decay in hundreds of τ_R, whereas a passive tracer would be smeared out in a few τ_R. Here, $\tau_R = 10\,\mu s$. The probability distribution ρ for measuring density n is strongly skewed towards low densities because the fluctuations are not random, but rather reflect the coherent holes.

A simple fluid model [17] shows that elliptical vortices can be in equilibrium with a weak imposed shear, but are elongated and destroyed by strong shear. Specifically, if the shear is prograde (*i.e.* in the vortex rotation direction), elliptical equilibria exist for all shear strengths; however, strong shear gives unphysically large elongations. If the shear is retrograde, equilibria exist only for weak shear.

Thus, in flows with strong negative shear (*i.e.* $\partial\omega_R/\partial r < 0$), such as Fig. 3 after $\approx 30\ \tau_R$, density clumps and shallow holes are sheared apart by the background flow, while relatively intense holes remain self-trapped. Measurements of the aspect ratios of these elliptical holes agree with the equilibria predicted for the measured shear [16]. Similar results have been seen for the stability of vortices in an applied shear field [18]. However, we also observe that the holes slowly drift outward (due to unknown effects) and are eventually destroyed.

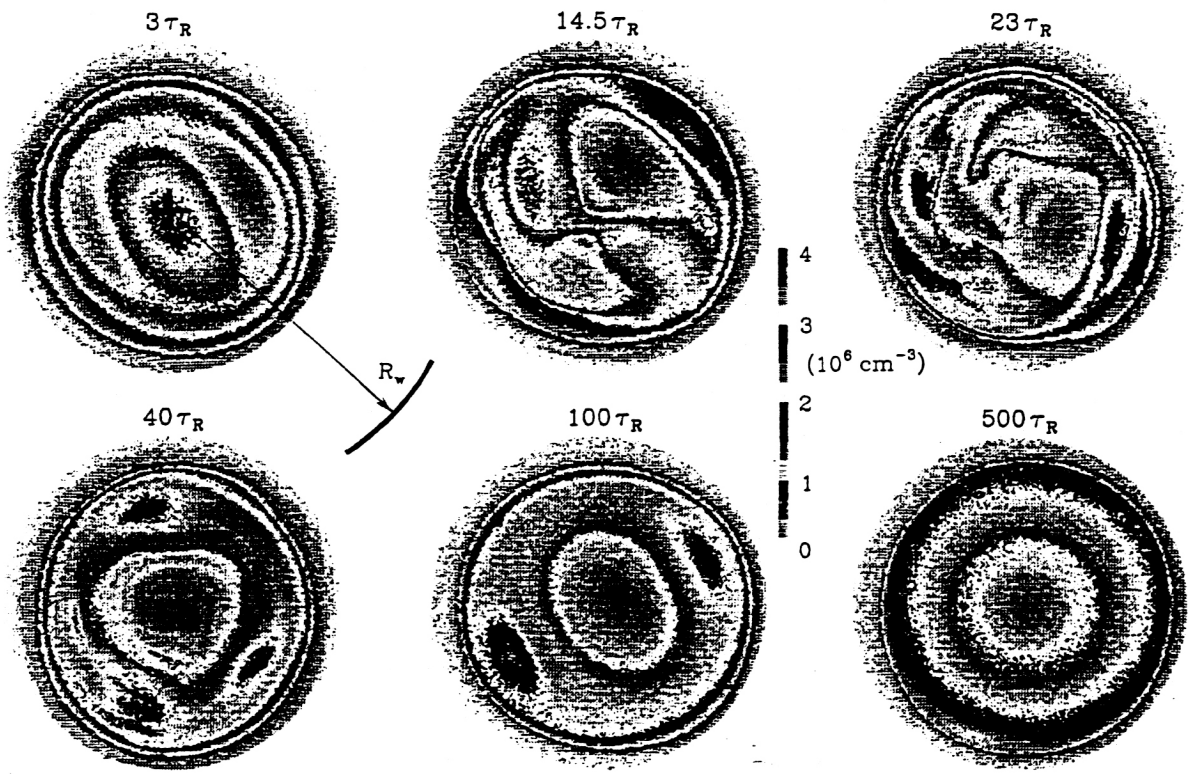

FIG. 3. Contours of the density (vorticity) during instability, vortex-driven transport, and relaxation to a meta-equilibrium state.

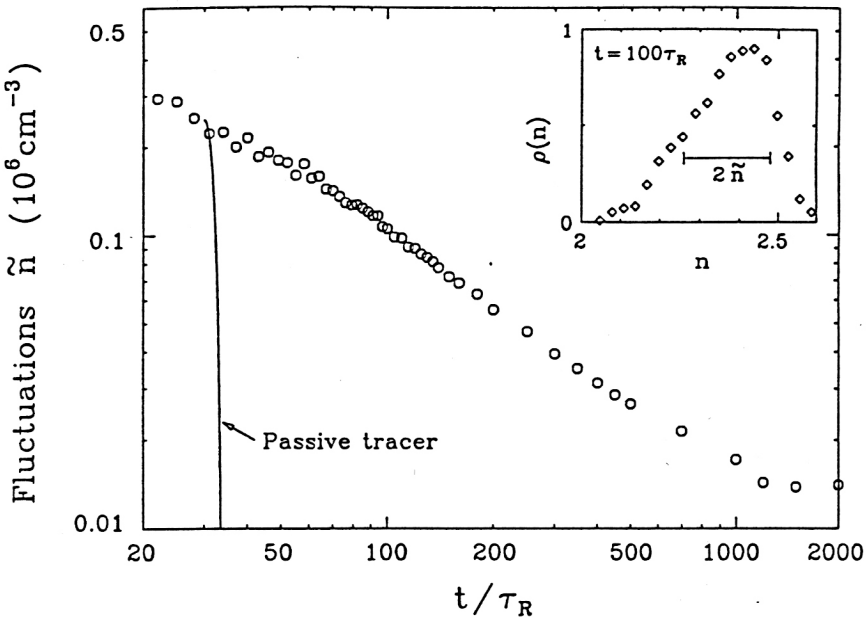

FIG. 4. Measured decay of fluctuations compared to passive tracer prediction, and measured non-Gaussian fluctuation distribution.

4. Minimum Enstrophy States States

Generally, the system relaxes to a low-noise meta-equilibrium state (MES). We generally observe that the MES is axisymmetric with a monotonically decreasing density profile, and lasts for about $10^4\ \tau_R$ before non-ideal effects cause it to evolve further. The total number of electrons, scaled angular momentum and scaled electrostatic energy, given by

$$N \equiv \int d^2\mathbf{r}\, n\ ,$$

$$P_\theta \equiv R_w^{-2} \int d^2\mathbf{r}\, (1-r^2)\, n/n_0\ ,$$

$$H_\phi \equiv -\tfrac{1}{2} R_w^{-2} \int d^2\mathbf{r}\, (n/n_0)\, (\phi/\phi_0)\ ,$$

are well conserved from the initial conditions to the MES [19]. Here, $n_0 \equiv N/R_w^2$, and $\phi_0 \equiv eN$. However, less robust "ideal" invariants such as enstrophy and mean-field entropy, given by

$$Z_2 \equiv \tfrac{1}{2} R_w^{-2} \int d^2\mathbf{r}\, (n/n_0)^2\ ,$$

$$S \equiv -R_w^{-2} \int d^2\mathbf{r}\, (n/n_0) \ln (n/n_0)\ ,$$

vary significantly, due to measurement coarse-graining or dissipation of small spatial scales.

We have compared the measured MES density profiles to various theories based on maximization of entropy or minimization of enstrophy [20]. We find that minimization of enstrophy accurately predicts the meta-equilibrium profiles for hollow initial conditions of moderate energy [19] such as shown in Fig. 3. These profiles are significantly different from the predictions of maximum entropy. The minimization is subject to constant N, P_θ, and H_ϕ, and to the physical constraint that $n \geq 0$. The explicit P_θ dependence of the solution is removed by rescaling the enstrophy as $\hat{Z}_2 \equiv 4\pi(1-P_\theta) Z_2$, and considering the excess energy

$$H_\phi^{\text{exc}} \equiv H_\phi - H_\phi^{\min}\ .$$

Here, $H_\phi^{\min} \equiv 1/4 - \tfrac{1}{2}\ln(2-2p_\theta)$ is the minimum energy possible for given N and P_θ, *i.e.* the energy of a uniform density column.

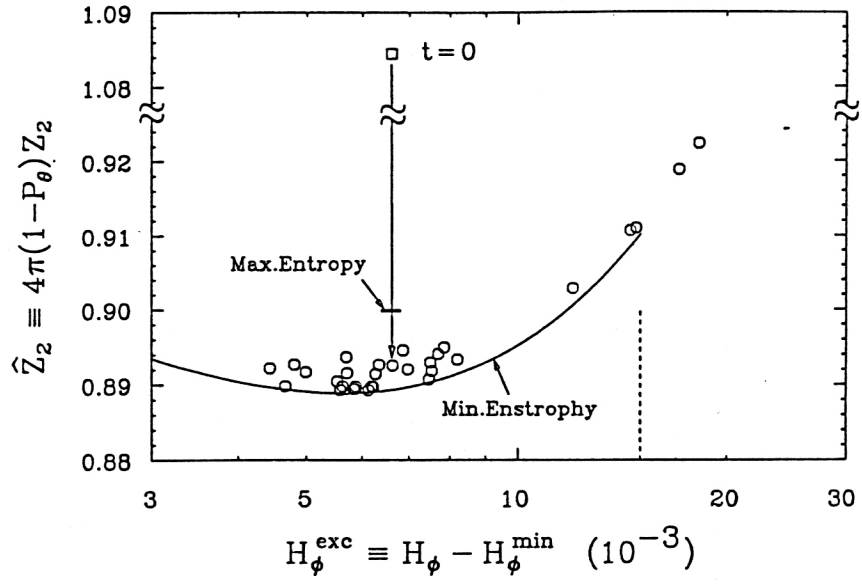

FIG. 5. Predicted (curve) and measured (points) enstrophy $\hat{Z}_2$ vs excess energy H_ϕ^{exc}.

Figure 5 shows the measured MES $\hat{Z}_2$ (circles) and the predicted minimum $\hat{Z}_2$ (curve) for a range of excess energies. Also shown is the value of $\hat{Z}_2$ which would be obtained from a maximum entropy MES for one evolution. Here, the experimental measurements are typically 2-3 times closer to the minimum enstrophy predictions than to the maximum entropy predictions, both in the measured Z_2 and in the measured profiles $n(r)$. For higher excess energies, this class of symmetric, monotonic solutions no longer exist, and several off-axis and non-monotonic profiles are possible [21].

5. Vortex Crystal States

We have also studied highly filamented, high excess energy initial conditions, which form 50-100 vortices, and then freely relax toward a 2D meta-equilibrium. Here, chaotic mutual advection and vortex merger are clearly important dynamical processes, and the final meta-equilibrium is typically strongly peaked on center. Surprisingly, this relaxation is sometimes halted when individual vortices settle into a stable, rotating crystalline pattern which lasts for thousands of rotation times.

Figure 6 shows the measured z-averaged electron density $n(r,\theta,t)$ at five times for two slightly different initial conditions: the upper sequence forms vortex crystals, whereas the lower sequence relaxes rapidly to a monotonically-decreasing profile [22]. The vortex crystal state consists of 5-11 individual vortices each 4–6 times the background vorticity, arranged in a lattice pattern which rotates with the background. That is, rods of enhanced electron density ($n \sim 7\times10^6\,\mathrm{cm}^{-3}$) are maintaining self-coherence and positions relative to each other for several seconds, while $\mathbf{E}\times\mathbf{B}$ drifting with a diffuse background ($n_B \sim 2\times10^6\,\mathrm{cm}^{-3}$). Vortex crystal states are repeatably observed over a range of filament bias voltages, but the characteristics of $n(r,\theta)$ required for these states are not yet understood. The lowest row in Fig. 6 shows selected patterns which have been observed.

Figure 7 shows the number of distinct vortices N_v, and the enstrophy Z_2 for the two sequences. In both sequences, the unstable filamentary initial condition forms $N_v = 50$–100 vortices of roughly equal circulation, after which N_v initially decreases as $N_v \sim t^{-\xi}$, with $\xi \approx 1$. This relaxation is generally consistent with a dynamical scaling based on conserved quantities

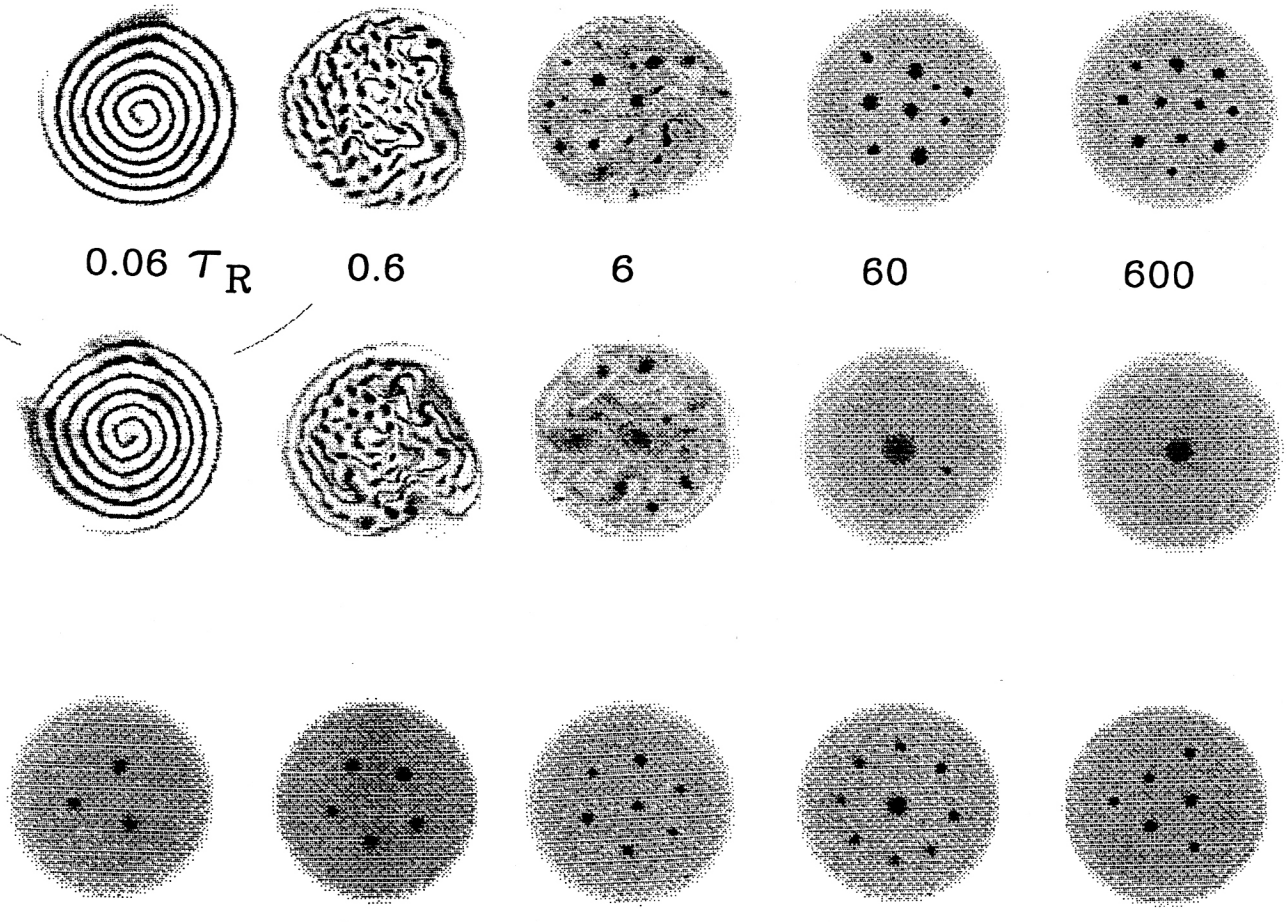

FIG. 6. Measured $n(r,\theta)$ at 5 times for two slightly different initial conditions, one of which forms vortex crystals; and 5 selected patterns which were observed.

in repeated vortex merger [23]. The observed ξ range from 0.4 to 1.1 as the initial conditions are varied, with 0.8 being commonly observed.

In the evolution of the top sequence in Fig. 6, the relaxation is arrested by the ''cooling'' of the chaotic vortex motions, with formation of vortex crystals by $10\,\tau_R$. (Here, $\tau_R = 170\,\mu$s.) The diamonds in Fig. 7 show that 8 to 10 distinct vortices survive for about $10^4\,\tau_R$. When the vortices all have about the same circulation, the patterns are quite regular, as seen at $600\,\tau_R$ in Fig. 6. After $10^4\,\tau_R$, N_v decreases to 1 as the individual vortices decay away in place. Other experimental images show that as N_v decreases, the remaining vortices re-adjust to a new rigidly rotating, symmetrically spaced pattern.

The measured integral quantities for both sequences are consistent with 2D inviscid motion on large scales and dissipation on fine scales. Experimentally, the circulation, angular momentum, and energy are robust invariants. In contrast, the enstrophy Z_2 is a ''fragile'' invariant, and initially decays a factor of 2 in both sequences. For the crystals sequence, Z_2 is constant from $10\tau_R$ until $10^4\tau_R$, at which time the individual vortices decay in place.

Reduction of the chaotic advective motions of the individual vortices is required to form the vortex crystal states. The average magnitude of the random velocities of the individual vortices, $|\delta V|$, decreases a factor of 6 between 2 τ_R and 100 τ_R for the crystals sequence, whereas only slight cooling is seen before $N_v = 1$ (and $|\delta V| = 0$ by definition) for the monotonic sequence [22].

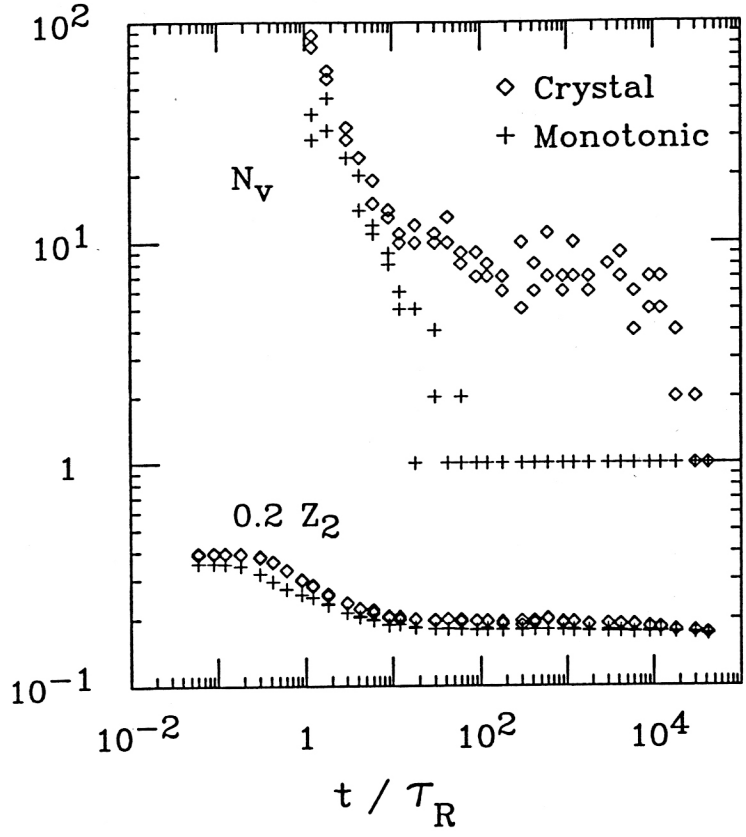

FIG. 7. Number of discrete vortices N_v and total enstrophy Z_2 versus time for two evolutions, one of which forms vortex crystals.

We believe this cooling and cessation of relaxation through mergers is a near-inviscid 2D fluid effect, *i.e.* independent of the details of the fine-scale dissipation [22]. It appears that the vortex cooling occurs due to an interaction between the individual vortices and the boundary of the background vorticity. A weak interaction would be described as the excitation of surface waves on the background, and these waves could be damped by direct or beat-wave spatial Landau damping as described above. For strong interactions and short wavelengths, this would correspond to entrainment and mixing of low vorticity regions from the edge of the column. A similar process may cause the negative vorticity "holes" to become symmetrically situated, as discussed above.

Many different symmetric crystal patterns have been observed, with 3–10 vortices. Apparently, there are many different "meta-equilibria" to which the system can evolve under near-inviscid 2D dynamics. Because of these attractors, the system does not evolve ergodically, and the final state cannot be predicted from statistics alone. Nor can this system be adequately approximated as point vortices punctuated by occasional merger events: the discrete vortex motion is non-Hamiltonian due to interaction with the background vorticity. In contrast, experiments on vortex dynamics without a background have shown frequencies and instability rates closely corresponding with point vortex theory [14].

6. Viscosity from Rotational Pumping

Eventually, diffusive or viscous effects cause the 2D meta-equilibrium to evolve further; this is seen in Fig. 7 as N_v and Z_2 decreasing after $10^4\tau_R$, which is 1.7 seconds. The physical process causing this slow evolution is not presently known, but a number of possibilities exist. Early electron plasma experiments established that the shear viscosity is

much greater than expected from local velocity scattering collisions [2]. Other experiments established that non-fluid diffusive effects arise from the end confinement potentials for high temperature plasmas [24]. Most recently, ''rotational pumping'' experiments have accurately characterized the viscosity which arises due to the end confinement potentials [25].

Rotational pumping is the process by which bulk transport arises from compressional (or ''second'') viscosity acting on length changes in the plasma column. The length changes are driven by $\mathbf{E}\times\mathbf{B}$ drift rotation in the presence of asymmetric end potentials. Consider a long plasma column that is contained axially with end potentials that vary azimuthally. As a flux tube of plasma undergoes $\mathbf{E}\times\mathbf{B}$ drift rotation about the center of the column, the length of the tube oscillates about some mean value, and the $p_{\|}dV$ work produces a corresponding oscillation in $T_{\|}$. In turn, the collisional relaxation of $T_{\|}$ toward $T_{\perp}$ produces a slow dissipation of electrostatic energy into heat and a consequent radial expansion (cross field transport) of the plasma. We call the mechanism rotational pumping, by analogy with magnetic pumping in tokamaks.

We have made detailed comparisons between theory and experiment for the case where the end asymmetries are produced by displacing an electron column a distance D off axis, that is, by exciting an $m=1$ diocotron mode. In this case, the cross field transport implies a damping of the mode. Because the trap itself is cylindrically symmetric, the canonical angular momentum of the plasma is conserved. Thus, the displacement of the column off-axis must decrease as the plasma expands. As derived by Crooks and O'Neil [26], the damping rate for a column with radius R_p and length L_p in a cylinder of radius R_w is given by

$$\gamma_{est} \approx 4\kappa^2 \nu_{\perp,\|} \frac{\lambda_D^2}{L_p^2} \frac{R_p^2}{R_w^2} (1-2R_p^2/R_w^2)^{-1} .$$

Here, the length change of a flux tube is estimated by $\delta L = \kappa D r/R_w$, with $\kappa \approx 2$. The damping rate is proportional to $(\delta L/L_p)^2$, and to the collisional equipartition rate $\nu_{\perp\|}$.

Interestingly, the magnetic field strength enters the damping rate only through the dependence of $\nu_{\perp,\|}$ on r_c/b where $r_c = \bar{v}/\Omega$ and $b = e^2/T$ is the distance of closest approach. Thus, as the field strength is increased (and r_c/b decreased), the damping rate is nearly independent of field strength until the regime of strong magnetization is reached (*i.e.*, $r_c/b < 1$) and then drops off dramatically.

Figure 8 shows the measured (points) and predicted (curves) rates as a function of temperature; the rates drop dramatically in accord with theory as T becomes small. To obtain quantitative agreement, the exact plasma end shapes from the 3D Poisson solutions must be used to obtain δL (solid curve); approximating the end shapes as above gives less accurate predictions (dotted curve).

Rotational pumping is the best-understood example of asymmetry-induced transport in these plasmas, and it dominates at high magnetic fields because it does not decrease with B. At lower fields, other viscous or diffusive processes may also be important. Fortunately, the wide separation of time scales between the 2D fluid motions and the 3D viscous effects allows the processes to be to be studied independently.

This work was supported by NSF Grant PHY94-21318, ONR Grant N00014-89-J-1714, and DOE Grant DE-FG03-85ER53199.

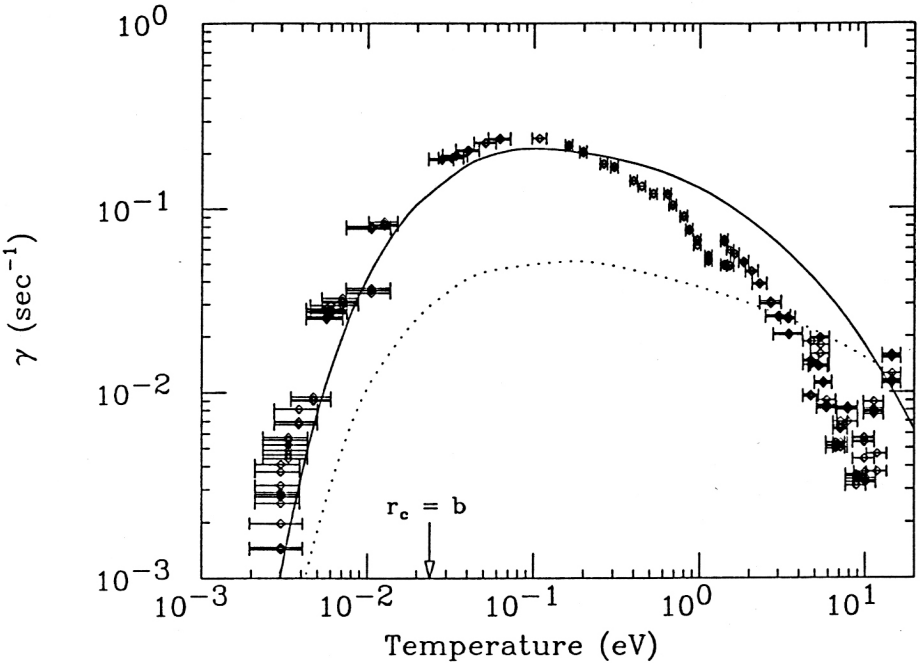

FIG. 8. Rotational pumping transport rate γ vs plasma temperature T.

References

1. C.F. Driscoll and K.S. Fine, "Experiments on Vortex Dynamics in Pure Electron Plasmas," Phys. Fluids **2**, 1359 (1990).
2. A. Hasegawa and K. Mima, "Pseudo 3D Turbulence in Magnetized Nonuniform Plasma," Phys. Fluids **21**, 87 (1978).
3. C.F. Driscoll, K.S. Fine and J.H. Malmberg, "Observation of Transport to Thermal Equilibrium in Pure Electron Plasmas," Phys. Rev. Lett. **60**, 1290 (1988).
4. W. Horton, J. Liu, J.D. Meiss and J.E. Sedlak, "Solitary Vortices in a Rotating Plasma," Phys. Fluids **29**, 1004 (1986).
5. T. Huld, A.H. Nielsen, H.L. Pecseli and J.J. Rasmussen, "Coherent Structures in 2D Plasma Turbulence," Phys. Fluids B **3**, 1609 (1991).
6. B. Song and A.K. Sen, "Flow-Shear Stabilization of Ion-Temperature-Gradient-Driven Instability in a Linear Machine," Phys. Rev. Lett. **72**, 92 (1994).
7. C.F. Driscoll, J.H. Malmberg, K.S. Fine, R.A. Smith, X.-P. Huang and R.W. Gould, "Growth and Decay of Turbulent Vortex Structures in Pure Electron Plasmas," Plasma Physics and Controlled Nuclera Fusion Research 1988, **3**, 507 (Vienna: IAEA, 1989).
8. C.F. Driscoll, "Observation of an Unstable $l = 1$ Diocotron Mode on a Hollow Electron Column," Phys. Rev. Lett. **64**, 645 (1990).
9. R.A. Smith and M.N. Rosenbluth, "Algebraic Instability of Hollow Electron Columns and Cylindrical Vortices," Phys. Rev. Lett. **64**, 649 (1990); R.A. Smith, "Effects of Electrostatic Confinement Fields and Finite Gyroradius on Instability of Hollow Electron Columns," Phys. Fluids B **4**, 287 (1992).
10. W. Kelvin, "On a Disturbing Infinity in Lord Rayleigh's Solution for Waves in a Plane Vortex Stratum," Nature **23**, 45 (1880).

11. R.H. Levy, "Diocotron Instability in Cylindrical Geometry," Phys. Fluids **8**, 1288 (1965); Phys. Fluids **11**, 920 (1968); R.J. Briggs *et al.*, "Landau Damping in Crossed-Field Electron Beams and Inviscid Shear Flow," Phys. Fluids **13**, 421 (1970).

12. N.S. Pillai and R.W. Gould, "Damping and Trapping in 2D Inviscid Fluids," Phys. Rev. Lett. **73**, 2849 (1994).

13. T.B. Mitchell, C.F. Driscoll and K.S. Fine, "Symmetrization of 2D Vortices by Beat-Wave Damping," *Phys. Rev. Lett.* **73**, 2196 (1994).

14. T.B. Mitchell, C.F. Driscoll and K.S. Fine, "Experiments on Stability of Equilibria of Two Vortices in a Cylindrical Trap," Phys. Rev. Lett. **71**, 1371 (1993).

15. K.S. Fine, C.F. Driscoll, J.H. Malmberg and T.B. Mitchell, "Measurements of Symmetric Vortex Merger," Phys. Rev. Lett. **67**, 588 (1991).

16. X.-P. Huang, K.S. Fine and C.F. Driscoll, "Coherent Vorticity Holes from 2D Turbulence Decaying in a Background Shear Flow," Phys. Rev. Lett. **74**, 4424 (1995); X.-P. Huang, Experimental Studies of Relaxation of 2D Turbulence in Magnetized Electron Plasma Columns, Ph.D. Thesis, UCSD (1993).

17. D.W. Moore and P.G. Saffman, "Aircraft Wake Turbulence and its Detection, 339 (New York: Plenum, 1971).

18. D.L. Eggleston, "Experimental Study of 2D Electron Vortex Dynamics in an Applied Irrotational Shear Flow," Phys. Plasmas **1**, 3850 (1994).

19. X.-P. Huang and C.F. Driscoll, "Relaxation of 2D Turbulence to a Meta-Equilibrium Near the Minimum Enstrophy State," Phys. Rev. Lett. **72**, 2187 (1994).

20. R.H. Kraichnan and D. Montgomery, "Two-Dimensional Turbulence," Rep. Prog. Phys. **43**, 547 (1980).

21. G. Sandler and D.H.E. Dubin, "Off-Axis and Haloed Equilibria from a Minimum Enstrophy Analysis of the Relaxation of 2-d Turbulence," in preparation.

22. K.S. Fine, A.C. Cass, W.G. Flynn and C.F. Driscoll, "Relaxation of 2D Turbulence to Vortex Crystals," Phys. Rev. Lett., submitted (1995).

23. G.F. Carnevale *et al.*, Phys. Rev. Lett. **66**, 2735 (1991); J.B. Weiss and J.C. McWilliams, Phys. Fluids A **5**, 608 (1993).

24. A.J. Peurrung and J. Fajans, "A Limitation to the Analogy Between Pure Electron Plasmas and 2D Inviscid Fluids," Phys. Fluids B **5**, 4295 (1993).

25. B.P. Cluggish and C.F. Driscoll, "Transport and Damping from Rotational Pumping in Magnetized Electron Plasmas," Phys. Rev. Lett. **74**, 4213 (1995); B.P. Cluggish, Experiments on Asymmetry-Induced Particle Transport in Magnetized, Pure Electron Plasma Columns, Ph.D. thesis, UCSD (1995).

26. S. Crooks and T.M. O'Neil, "Rotational Pumping and Damping of the $m = 1$ Diocotron Mode," *Phys. Plasmas* **2**, 355 (1995).